Microwave Response of Superconducting $YBa_2Cu_3O_{7-\delta}$ Nanowire Bridges Sustaining the Critical Depairing Current: Evidence of Josephson-like Behavior

S. Nawaz,[1] R. Arpaia,[1,2] F. Lombardi,[1] and T. Bauch[1]

[1]*Deptartment of Microtechnology and Nanoscience, Quantum Device Physics Laboratory, Chalmers University of Technology, SE-412 96 Göteborg, Sweden*

[2]*CNR-SPIN, Dipartimento di Scienze Fisiche, Università degli Studi di Napoli Federico II, I-80126 Napoli, Italy*

(Received 25 September 2012; published 18 April 2013)

We have investigated the zero-field critical supercurrent of $YBa_2Cu_3O_{7-\delta}$ bridges patterned from 50 nm thick films as a function of bridge width, ranging from 2 μm to 50 nm. The critical current density monotonically increases for decreasing bridge width even for widths smaller than the Pearl length. This behavior is accounted for by considering current crowding effects at the junction between the bridge and the wider electrodes. Comparison to numerical calculations of the current distributions in our bridge geometries of various widths yields a (local) critical current density at 4.2 K of 1.3×10^8 A/cm^2, the Ginzburg Landau depairing current density. The observation of up to 160 Shapiro-like steps in the current voltage characteristics under microwave irradiation substantiates the pristine character of our nanobridges with cross sections as small as 50×50 nm^2.

DOI: 10.1103/PhysRevLett.110.167004 PACS numbers: 74.78.Na, 74.25.Sv, 74.72.Gh

Recent advances in nanopatterning techniques have paved the way for studying fundamental aspects of superconductivity on the nanoscale. The expected suppression of superconductivity and the search for quantum coherent phase slip events in superconducting nanowires with cross-sectional dimension on the nanometer scale [1] has triggered a variety of exciting experiments [2–4]. The study of nanopatterned high critical temperature superconductors (HTSs) in the form of nanorings [5,6], nanobridges [7,8], and nanodots is expected to elucidate the unresolved puzzle of the microscopic mechanism leading to superconductivity in these unconventional materials as recently demonstrated in a nanometer sized HTS island [9]. Nanoscale superconductors also allow for new exciting developments towards quantum-limited sensors such as superconducting nanowire single photon detectors [10] and nanoscale superconducting quantum interference devices (nanoSQUIDs) with unprecedented flux sensitivity [11,12]. The realization of wires with highly homogeneous superconducting properties is of essential importance to enable fundamental studies and operational reproducible devices. While this issue is within the reach of available nanotechnologies for conventional superconductors [1], it still represents a challenge for cuprate HTSs. The chemical instability of these materials, mostly related to oxygen outdiffusion, and the extreme sensitivity to defects and disorder due to the very short superconducting coherence length ξ (of the order of 2 nm), do represent real issues in establishing reliable nanofabrication routines. Indeed, the nanopatterning of HTS materials has been a longstanding challenge.

An excellent method for assessing the quality and homogeneity of nanopatterned superconducting bridges is the measurement of the maximum supercurrent density J_c that in bridges with cross sections smaller than the London penetration depth, λ_L, should be given by the theoretically expected Ginzburg Landau (GL) depairing limit, $J_{GL} = \Phi_0/3\sqrt{3}\pi\mu_0\lambda_L^2\xi$, with $\Phi_0 \simeq 2 \times 10^{-15}$ T m^2 the superconducting flux quantum, and μ_0 the vacuum permeability. J_c is extremely sensitive to any inhomogeneity in the superconducting properties along the bridge and to the film edge roughness [13–15]. Reaching the theoretical GL depairing limit is an issue even for conventional superconductors [16]. Up to now, all experimental values on critical current densities in cuprate HTS nanobridges reported in literature show a wide spread and especially a reduction of the critical current density, J_c, when approaching lateral dimensions on the 100 nm scale [15,17]. This is indicative of a degradation of the superconducting properties. Moreover, the reported critical current densities are still below the theoretically expected GL depairing limit.

In this Letter we report on an experimental and numerical study of the critical current density, $J_c(w)$, in $YBa_2Cu_3O_{7-\delta}$ (YBCO) nanobridges as a function of bridge width, w, showing that the critical current in our nanobridges is only limited by the GL depairing current density. This limit, never reached earlier for HTS materials, raises also the question about the possibility to establish in such nanostructures a nonlinear supercurrent phase relation so as to detect all the Josephson-like related phenomenology as predicted for superconducting nanobridges with dimensions smaller than the Pearl length [18,19]. We have approached this issue by studying the microwave response of the electronic transport through our nanobridges.

In contrast to previous works, which analyze the experimental data by treating the bridges as infinitesimal long bridges [13,14] [see Fig. 1(a)], here we take into account the influence of the wide electrodes, connecting the

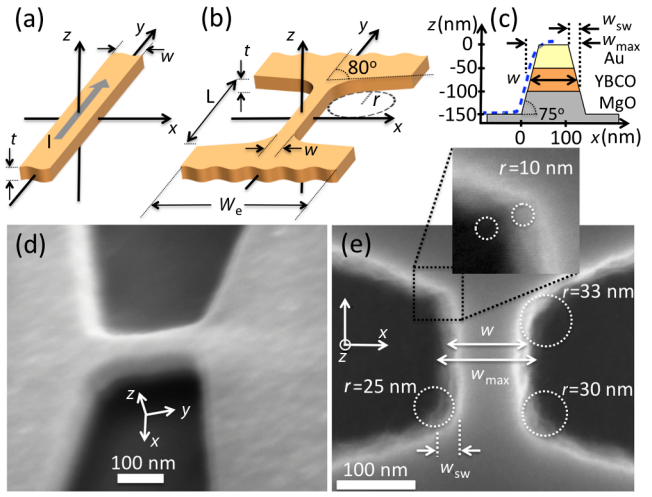

FIG. 1 (color online). (a) Sketch of an infinite long bridge of thickness t and width w. The current in the bridge flows only along the y direction. (b) Sketch of a bridge of thickness t, width w, and length L connected to wide electrodes. (c) Sketch of the cross section of a patterned bridge. The dashed line is a typical atomic force microscope (AFM) line scan along the cross section of a nanobridge. The slope of the bridge side walls is $\sim 75°$. The lateral extension of the YBCO/Au bridge side walls is given by $w_{sw} \simeq 100\ \text{nm}/\tan 75° = 26$ nm. (d) Scanning electron microscopy (SEM) image of a 200 nm long and 75 nm wide bridge (45° tilted stage). (e) SEM image of a 200 nm long and 100 nm wide YBCO/Au bridge (top view). The width of the Au/YBCO bridge side wall is $w_{sw} \simeq 25$ nm [see also panel (c)]. The dotted circles indicate the bending radii of the inner corners. The inset is a magnification of the upper left inner corner. The two dotted circles denote the bending radii in the Au (right circle) and YBCO film (left circle), respectively.

nanobridge to the biasing circuit, on the critical current density [see Fig. 1(b)]. Only recently the critical current reduction due to turns and corners in superconducting nanowire structures with lateral dimensions much smaller than the Pearl length, $\lambda_P = \lambda_L^2/t$, with t the film thickness, was studied theoretically [20] and the first experimental evidence was found in conventional superconductors [21,22]. However, since our bridges have widths ranging far below and above the Pearl length and are connected to electrodes much wider than the Pearl length, we instead apply numerical methods for calculating the current distributions in our structures.

We fabricated 200 nm long nanobridges of various widths (50 nm to 2 μm) from 50 nm thick YBCO films. The YBCO film was grown by pulsed laser deposition on a (110) MgO substrate. A 50 nm Au film was deposited *ex situ* on top of the YBCO acting as a protective layer for the YBCO film during the patterning process. The patterning of HTS films on the nanoscale is an extremely challenging task. The most viable technology is the pattern transfer through a hard mask using Ar ion etching [23–25]. However, the detrimental effect of the Ar ion etching on the exposed surfaces of YBCO causes damaged layers having reduced superconducting or even insulating properties [26]. We drastically improved the nanopatterning of YBCO obtaining nanobridges without any deterioration of the superconducting properties, as we will show below. This has been achieved by using electron beam lithography in combination with a 100 nm thick carbon mask and a very gentle ion milling to define the nanobridges [23,27]. Here we used an ion acceleration voltage close to the threshold value of $V \simeq 300$ V, below which YBCO is not etched. Moreover we have used the lowest ion beam current density $J_{Ar^+} = 0.08\ \text{mA/cm}^2$ that allowed the ignition of the plasma in our milling system. The total etching time is such that we also ion-mill approximately 50 nm into the substrate. This assures the removal of any redeposited YBCO in the vicinity of the nanobridge. Scanning electron microscopy (SEM) images of typical nanobridges are shown in Figs. 1(d) and 1(e). An atomic force microscope (AFM) line scan along the cross section of a typical nanobridge together with a sketch of a bridge cross section is shown in Fig. 1(c). We define the width of a bridge, w, as the bridge width at half the YBCO film thickness [see Fig. 1(c)]. The width of the YBCO/Au bridge side walls determined from AFM, $w_{sw} \simeq 26$ nm [see Fig. 1(c)], is in good agreement with the one determined from SEM [Fig. 1(e)]. Thus, we can determine the width of a bridge from SEM, $w = w_{max} - w_{sw}/2$, where w_{max} is the width of the bridge at the interface between YBCO and MgO [see Fig. 1(e)] [28]. The electrical transport measurements of our nanobridges were performed in a ^{3}He cryostat. The current voltage characteristics (IVCs) were recorded using a four-point measurement scheme in current bias mode. All nanobridges exhibit critical temperatures similar to that of the wide electrodes, $T_c \simeq 85$ K, differing not more than 1 K (data not shown). The critical current of the bridge I_c^{ex} is determined from the IVCs as the bias current above which the bridge undergoes a transition from the zero voltage state to the finite voltage state. Here we use a voltage criterion of 2 μV. From the critical current values we can calculate the average critical current density $J_c^{ex} = I_c^{ex}/A_{cr}$ for each bridge, where $A_{cr} = w \times t$ is the smallest cross-sectional area of the bridge, which we determined by SEM imaging.

At first we discuss the width dependence of the critical current density, $J_c(w)$, in infinite long (type II) superconducting bridges, i.e., neglecting the influence of wide electrodes [see Fig. 1(a)]. We limit ourselves to the thin film case ($t < \lambda_L$) since the thickness of our c-axis films ($t = 50$ nm) is well below the in-plane London penetration depth $\lambda_L^{ab} \simeq 150$–$220$ nm [15]. Thus we can neglect current components parallel to the z direction and assume a homogeneous current distribution throughout the whole film thickness. In addition, all the lateral dimensions of our bridges are larger than the superconducting coherence length $\xi \simeq 1.5$–2 nm. Here we consider the case of zero

externally applied magnetic field. For bias currents smaller than the critical current, I_c, a finite edge barrier prevents vortices from entering the bridge [29–37]. Increasing the bias current from zero to a finite value gradually reduces this edge barrier. For the bias current approaching the critical current the barrier is eventually completely suppressed at a distance on the order of the coherence length from the bridge edge, allowing vortices to enter the bridge. The resulting vortex motion across the bridge, driven by the Lorentz force, causes a finite voltage drop along the bridge. The value of the critical supercurrent depends on the detailed in-plane current distribution $\vec{j}(x, y)$ in the bridge, which for $\xi \ll \lambda_L$ is given by the Maxwell and London equations describing the Meissner state [38]:

$$\mu_0 \vec{\nabla} \times (\lambda^2 \cdot \vec{j}) + \vec{B} = 0; \qquad \vec{\nabla} \times \vec{B} = \mu_0 \vec{j}, \tag{1}$$

where μ_0 is the vacuum permeability, λ^2 the material specific London penetration depth (squared) tensor, and $\vec{B}$ the magnetic field solely generated by the transport currents. We calculated the current distributions $j_y(x)$ for various bridge widths by numerically solving Eq. (1) on a geometry depicted in Fig. 1(a). In the inset of Fig. 2(a) we show $j_y(x)$ for three different bridge widths, $w = 0.2\lambda_P$, $2\lambda_P$ and $20\lambda_P$, respectively. One can clearly observe that the current density at the edges of a bridge with $w > \lambda_P$ is enhanced compared to the average value $\bar{J} = \int j_y(x)dx/w$. When ramping up the bias current applied to a bridge the critical supercurrent is reached once the local current density at the edges of the bridge $j_y(\pm w/2)$ equals a value close to the depairing current density, J_{GL} [31,34]. At this point the edge barrier is suppressed and vortices can enter the bridge, causing a transition from the zero voltage state to the finite voltage state. Thus, from the local current density at the edges $j_y(\pm w/2)$ and the average current density $\bar{J}$ one can compute the average critical current density as a function of width:

$$\bar{J}_c(w) = J_S \bar{J}/j_y(\pm w/2), \tag{2}$$

where J_S is approximately the depairing value, $J_S \simeq J_{\mathrm{GL}}$. In Fig. 2(a) we show the resulting normalized average critical current density $\bar{J}_c(w)/J_S$ as a function of bridge width.

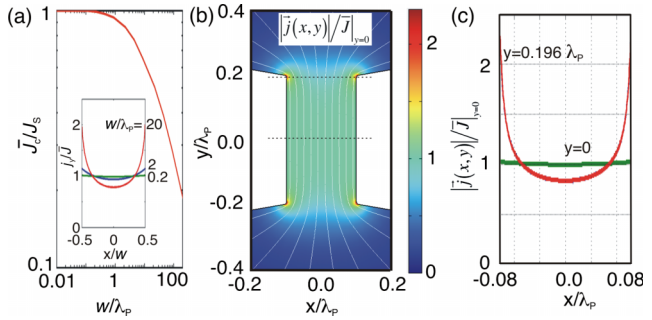

FIG. 2 (color online). (a) Calculated normalized average critical current density as a function of bridge width for an infinitesimal long bridge. The inset shows the local current density in the y direction across the bridge normalized to the average current density $\bar{J}$ for three different values of the normalized bridge width $w/\lambda_P = 20$, 2, and 0.2. (b) Calculated absolute value of the local current density normalized to the average current density at $y = 0$. The width of the bridge is $w = 0.2\lambda_P$ and the length $L = 0.4\lambda_P$. The inner corners have a bending radius $r = 0.05w$. The width and the length of the electrodes are $10\lambda_P$ and $12\lambda_P$, respectively. A constant current density is injected at the end of one electrode at $y = 12.2\lambda_P$ and extracted at the other electrode at $y = -12.2\lambda_P$ (not shown). The white lines indicate the path of the current flow. (c) Line cuts of the current density at $y = 0$ and $y = 0.196\lambda_P$ indicated as dashed lines in (b).

In Fig. 3(a) we show the expected $\bar{J}_c(w)$ for infinite long bridges [39] (solid line) together with the experimentally determined critical current densities J_c^{ex} (symbols) as a function of bridge width. One can clearly see that J_c^{ex} does not saturate for a bridge width below the Pearl length $\lambda_P \simeq 800$ nm. The discrepancy between the experimental data and the expected behavior for infinite long bridges, however, can be explained by taking into account the influence of the on-chip (wide) electrodes connecting the bridge to the bias circuitry [see Fig. 1(b)]. In this case the current injection from the wide electrodes into the thin bridge causes current crowding at the inner corners of the junction between the bridge and electrode; i.e., the local current density at the inner corners is enhanced compared to the average current density at the center of the bridge [20,41], $\bar{J}|_{y=0} = \int j_y(x, y = 0)dx/w$. To illustrate the current crowding we show in Fig. 2(b) a calculated local current density in a typical geometry depicted in Fig. 1(b) by solving numerically Eq. (1). Figure 2(c) shows two line cuts of Fig. 2(b): one at the center of the bridge and the other close to the electrodes. One can clearly see the enhanced current density at the inner corners of the bridge geometry even though the width of the bridge is much smaller than the Pearl length, $w = 0.2\lambda_P$. The average critical current density in this case can be computed from the numerically determined current distributions in the following way:

$$\bar{J}_c(w) = J_S \bar{J}|_{y=0}/j_{\max}, \tag{3}$$

where $j_{\max}$ is the maximum value of the current density located at the inner corners. Depending on the ratio between the inner corner bending radius and the bridge width, the current crowding can strongly reduce the average critical current density of a bridge below its infinite long bridge limit even for bridge widths smaller than the Pearl length. The dashed and dotted lines in Fig. 3(a) are the numerically calculated average critical current densities using Eq. (3) for bending radii of the inner corners $r_1 = 40$ nm and $r_2 = 10$ nm, respectively. The values for the bending radii comprise the range we obtain by our lithography process for nominally 80° corners [see Fig. 1(e)]. For all the numerically determined $J_c(w)$

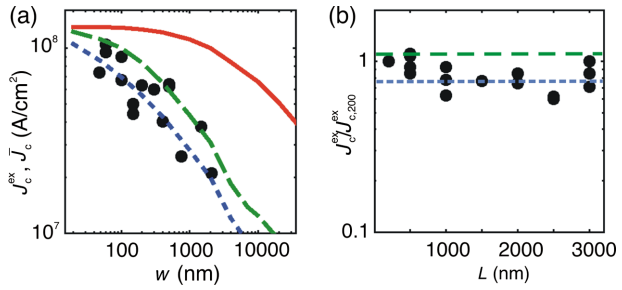

FIG. 3 (color online). (a) Critical current density as a function of bridge width measured at 4.2 K (symbols). The solid line is the numerically calculated critical current density for an infinite long bridge using Eq. (2). The dashed and dotted lines are the numerically calculated critical current densities using Eq. (3) for 200 nm long bridges connected to wide electrodes with inner corner radii $r_1 = 40$ nm and $r_2 = 10$ nm, respectively. (b) Critical current density of 100 nm wide nanobridges as a function of bridge length normalized to the value for $L = 200$ nm, $J_{c,200}^{ex}$, measured at $T = 4.2$ K. The dashed and dotted lines indicate the expected range of critical currents due to current crowding effects assuming $r = 40$ nm and $r = 10$ nm, respectively.

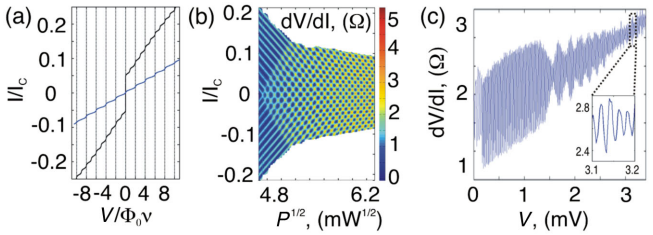

FIG. 4 (color online). Shapiro-like steps. (a) Current voltage characteristic at two applied microwave powers (source output), $P = 13$ dBm (black line) and $P = 16$ dBm (blue line). (b) Differential resistance map as a function of applied microwave amplitude (at source output) and bias current. The dark blue regions correspond to the Shapiro-like (current) steps. (c) Differential resistance as a function of voltage at a fixed microwave power $P = 14.5$ dBm. The inset shows a close-up of the Shapiro-like steps. In all three panels the temperature is $T = 4.2$ K and the applied microwave frequency $\nu = 10.13$ GHz.

dependencies we used fixed values for the Pearl length, $\lambda_P = 800$ nm, and $J_S = 1.3 \times 10^8$ A/cm^2. The agreement between experimental data and the current crowding model is indeed very good. Moreover the value of the local critical current density J_S used to fit our measurements is very close to the maximum theoretical depairing current density for YBCO. Figure 3(b) shows the critical current density measured at $T = 4.2$ K for 100 nm wide bridges as a function of bridge length. The length independence of the critical current density rules out the presence of redeposited YBCO in the vicinity of the bridges, which may possibly lead to an overestimation of J_c^{ex}. It is worth noting that the critical current density of a nanobridge connected to wide electrodes approaches the depairing value only for a width smaller than half the bending radius of the inner corners [see dashed line in Fig. 3(a)] similar to the result reported in Ref. [20].

We furthermore studied the ac Josephson-like effect in our smallest bridges with cross section 50×50 nm^2. If a superconducting nanobridge having dimensions smaller than the Pearl length is exposed to a microwave field, current steps in the IVC may appear at specific voltage values $V_n = n\nu\Phi_0$, where n is an integer, ν is the applied microwave frequency, and V is the voltage drop along the bridge [18,42]. These steps appear due to the synchronization of the coherent motion of Abrikosov vortices to the microwave radiation frequency by phase locking. Such current steps are similar to Shapiro steps observable in the IVCs of Josephson tunnel junctions when an external microwave field phase locks with the Josephson oscillations at finite voltages [43]. In Fig. 4(a) we show the measured IVCs under microwave irradiation ($\nu = 10.13$ GHz) for two different applied microwave powers. The Shapiro-like (current) steps occur at integer multiples of $\nu\Phi_0$. A differential resistance map of the nanobridge as a function of bias current and applied microwave amplitude is shown in Fig. 4(b). The periodic modulation of the current steps with the applied microwave amplitude gives a strong indication of the existence of an effective periodic current phase relation in the nanobridges [44]. The observation of up to 160 Shapiro-like steps, shown in Fig. 4(c), further corroborates the excellent quality of our bridges since any inhomogeneity in the superconducting properties would inhibit the coherent motion of Abrikosov vortices [18].

In conclusion we have performed a systematic study of the critical current of YBCO nanobridges as a function of lateral width ranging from 2 μm to 50 nm. All our bridges can be characterized by a (local) critical current density approaching the Ginzburg Landau depairing critical current density, 1.3×10^8 A/cm^2, down to cross sections of 50×50 nm^2. The observed current crowding effect in our nanobridges that manifests as an increase in J_c by reducing the nanobridge width, for width less than the Pearl length, has strong implications for the design of superconducting nanowire single photon detectors where a homogeneous current density along the whole bridge is essential for improving photon detection sensitivity [10].

This work has been partially supported by the Swedish Research Council (VR) and the Knut and Alice Wallenberg Foundation (KAW).

[1] A. Bezryadin, J. Phys. Condens. Matter **20**, 043202 (2008).
[2] J. E. Mooij and Y. V. Nazarov, Nat. Phys. **2**, 169 (2006).
[3] O. V. Astafiev, L. B. Ioffe, S. Kafanov, Y. A. Pashkin, K. Y. Arutyunov, D. Shahar, O. Cohen, and J. S. Tsai, Nature (London) **484**, 355 (2012).
[4] K. Y. Arutyuonov, T. T. Hongisto, J. S. Lehtinen, L. I. Leino, and A. L. Vasiliev, Sci. Rep. **2**, 293 (2012).

[5] I. Sochnikov, A. Shaulov, Y. Yeshurun, G. Logvenov, and I. Bosovic, Nat. Nanotechnol. **5**, 516 (2010).

[6] F. Carillo, G. Papari, D. Stornaiuolo, D. Born, D. Montemurro, P. Pingue, F. Beltram, and F. Tafuri, Phys. Rev. B **81**, 054505 (2010).

[7] P. Mohanty, J. Y. T. Wei, V. Ananth, P. Morales, and W. Skocpol, Physica (Amsterdam) **408–410C**, 666 (2004).

[8] J. A. Bonetti, D. S. Caplan, D. J. Van Harlingen, and M. B. Weissman, Phys. Rev. Lett. **93**, 087002 (2004).

[9] D. Gustafsson, D. Golubev, M. Fogelström, T. Claeson, S. Kubatkin, T. Bauch, and F. Lombardi, Nat. Nanotechnol. **8**, 25 (2013).

[10] H. Bartolf, A. Engel, A. Schilling, K. Il'in, M. Siegel, H. W. Hübers, and A. Semenov, Phys. Rev. B **81**, 024502 (2010).

[11] C. P. Foley and H. Hilgenkamp, Supercond. Sci. Technol. **22**, 064001 (2009).

[12] J. Gallop, Supercond. Sci. Technol. **16**, 1575 (2003).

[13] S. Tahara, S. M. Anlage, J. Halbritter, C.-B. Eom, D. K. Fork, T. H. Geballe, and M. R. Beasley, Phys. Rev. B **41**, 11 203 (1990).

[14] W. A. Jones, P. N. Barnes, M. J. Mullins, F. J. Baca, R. L. S. Emergo, J. Wu, T. J. Haugan, and J. R. Clem, Appl. Phys. Lett. **97**, 262503 (2010).

[15] G. Papari, F. Carillo, D. Stornaiuolo, L. Longobardi, F. Beltram, and F. Tafuri, Supercond. Sci. Technol. **25**, 035011 (2012).

[16] K. Xu, P. Cao, and J. R. Heath, Nano Lett. **10**, 4206 (2010).

[17] H. Assink, A. J. M. Harg, C. M. Schep, N. Y. Chen, D. Marel, P. Hadley, E. W. J. M. Drift, and J. E. Mooij, IEEE Trans. Appl. Supercond. **3**, 2983 (1993).

[18] K. K. Likharev, Zh. Eksp. Teor. Fiz. **61**, 1700 (1972) [Sov. Phys. JETP **34**, 906 (1972)].

[19] K. K. Likharev, Rev. Mod. Phys. **51**, 101 (1979).

[20] J. R. Clem and K. K. Berggren, Phys. Rev. B **84**, 174510 (2011).

[21] H. L. Hortensius, E. F. C. Driessen, T. M. Klapwijk, K. K. Berggren, and J. R. Clem, Appl. Phys. Lett. **100**, 182602 (2012).

[22] D. Henrich, P. Reichensperger, M. Hofherr, J. M. Meckbach, K. Il'in, M. Siegel, A. Semenov, A. Zotova, and D. Y. Vodolazov, Phys. Rev. B **86**, 144504 (2012).

[23] D. Gustafsson, F. Lombardi, and T. Bauch, Phys. Rev. B **84**, 184526 (2011).

[24] D. Stornaiuolo, G. Rotoli, K. Cedergren, D. Born, T. Bauch, F. Lombardi, and F. Tafuri, J. Appl. Phys. **107**, 113901 (2010).

[25] D. Gustafsson, H. Pettersson, B. Iandolo, E. Olsson, T. Bauch, and F. Lombardi, Nano Lett. **10**, 4824 (2010).

[26] F. Herbstritt, T. Kemen, A. Marx, and R. Gross, J. Appl. Phys. **91**, 5411 (2002).

[27] S. Nawaz, R. Arpaia, T. Bauch, and F. Lombardi (to be published).

[28] From the normal resistance of bare YBCO nanobridges (after removal of the gold capping layer) we obtain a sheet resistance of 20 Ω slightly above Tc corresponding to a resistivity $\rho \simeq 100\ \mu\Omega$cm, which is a typical value for thin YBCO films.

[29] C. P. Bean and Livingston, Phys. Rev. Lett. **12**, 14 (1964).

[30] M. Y. Kupriyanov and K. K. Likharev, Fiz. Tverd. Tela (Leningrad) **16**, 2829 (1974) [Sov. Phys. Solid State **16**, 1835 (1975)].

[31] L. G. Aslamazov and S. V. Lempitsky, Zh. Eksp. Teor. Fiz. **84**, 2216 (1983) [Sov. Phys. JETP **57**, 1291 (1983)].

[32] M. Benkraouda and J. R. Clem, Phys. Rev. B **58**, 15 103 (1998).

[33] G. M. Maksimova, Phys. Solid State **40**, 1607 (1998).

[34] D. Y. Vodolazov, I. L. Maksimov, and E. H. Brandt, Europhys. Lett. **48**, 313 (1999).

[35] A. A. Elistratov, D. Y. Vodolazov, I. L. Maksimov, and J. R. Clem, Phys. Rev. B **66**, 220506(R) (2002).

[36] A. Gurevich and V. M. Vinokur, Phys. Rev. Lett. **100**, 227007 (2008).

[37] L. N. Bulaevskii, M. J. Graf, C. D. Batista, and V. G. Kogan, Phys. Rev. B **83**, 144526 (2011).

[38] M. M. Khapaev, Supercond. Sci. Technol. **10**, 389 (1997).

[39] Our result coincides, within a few percent, with the analytical expression for $\bar{J}_c(w)$ in the infinite long bridge case presented in Ref. [40].

[40] B. L. T. Plourde, D. J. Van Harlingen, D. Y. Vodolazov, R. Besseling, M. B. S. Hesselberth, and P. H. Kes, Phys. Rev. B **64**, 014503 (2001).

[41] F. B. Hagedorn and P. M. Hall, J. Appl. Phys. **34**, 128 (1963).

[42] L. G. Aslamazov and A. I. Larkin, Zh. Eksp. Teor. Fiz. **68**, 766 (1975) [Sov. Phys. JETP **41**, 381 (1975)].

[43] S. Shapiro, Phys. Rev. Lett. **11**, 80 (1963).

[44] M. H. Bae, R. C. Dinsmore, T. Aref, M. Brenner, and A. Bezryadin, Nano Lett. **9**, 1889 (2009).